Title
Combined melatonin and poricoic acid A inhibits renal fibrosis through modulating the interaction of Smad3 and β-catenin pathway in AKI-to-CKD continuum.

Authors
Chen, Dan-Qian
Cao, Gang
Zhao, Hui
et al.

Publication Date
2019

DOI
10.1177/2040622319869116

Peer reviewed

Ther Adv Chronic Dis
2019, Vol. 10: 1–19
DOI: 10.1177/2040622319869116

Combined melatonin and poricoic acid A inhibits renal fibrosis through modulating the interaction of Smad3 and β-catenin pathway in AKI-to-CKD continuum

Dan-Qian Chen, Gang Cao, Hui Zhao, Lin Chen, Tian Yang, Ming Wang, Nosratola D. Vaziri, Yan Guo and Ying-Yong Zhao

Abstract

Background: Acute kidney injury (AKI) is one of the major risk factors for progression to chronic kidney disease (CKD) and renal fibrosis. However, effective therapies remain poorly understood. Here, we examined the renoprotective effects of melatonin and poricoic acid A (PAA) isolated from the surface layer of *Poria cocos*, and investigated the effects of combined therapy on the interaction of TGF-β/Smad and Wnt/β-catenin in a rat model of renal ischemia-reperfusion injury (IRI) and hypoxia/reoxygenation (H/R) or TGF-β1-induced HK-2 cells.

Methods: Western blot and immunohistochemical staining were used to examine protein expression, while qRT-PCR was used to examine mRNA expression. Coimmunoprecipitation, chromatin immunoprecipitation, RNA interference, and luciferase reporter gene analysis were employed to explore the mechanisms of PAA and melatonin's renoprotective effects.

Results: PAA and combined therapy exhibited renoprotective and antifibrotic effects, but the underlying mechanisms were different during AKI-to-CKD continuum. Melatonin suppressed Smad-dependent and Smad-independent pathways, while PAA selectively inhibited Smad3 phosphorylation through distrupting the interactions of Smad3 with TGFβRI and SARA. Further studies demonstrated that the inhibitory effects of melatonin and PAA were partially depended on Smad3, especially PAA. Melatonin and PAA also inhibited the Wnt/β-catenin pathway and its profibrotic downstream targets, and PAA performed better. We further determined that IRI induced a nuclear Smad3/β-catenin complex, while melatonin and PAA disturbed the interaction of Smad3 and β-catenin, and supplementing with PAA could enhance the inhibitory effects of melatonin on the TGF-β/Smad and Wnt/β-catenin pathways.

Conclusions: Combined melatonin and PAA provides a promising therapeutic strategy to treat renal fibrosis during the AKI-to-CKD continuum.

Keywords: melatonin, poricoic acid A, renal fibrosis, renal ischemia-reperfusion injury, TGF-β/Smad, Wnt/β-catenin

Received: 28 February 2019; revised manuscript accepted: 22 July 2019.

Correspondence to:
Ying-Yong Zhao
Faculty of Life Science & Medicine, Northwest University, No. 229 Taibai North Road, Xi'an, Shaanxi 710069, China
zyy@nwu.edu.cn; zhaoyybr@163.com

Dan-Qian Chen
Hui Zhao
Lin Chen
Tian Yang
Ming Wang
Faculty of Life Science & Medicine, Northwest University, Xi'an, Shaanxi, China

Gang Cao
School of Pharmacy, Zhejiang Chinese Medical University, Hangzhou, China

Nosratola D. Vaziri
Division of Nephrology and Hypertension, School of Medicine, University of California Irvine, CA, USA

Yan Guo
Faculty of Life Science & Medicine, Northwest University, Shaanxi, China

Department of Internal Medicine, University of New Mexico, Comprehensive Cancer Center, Albuquerque, NM, USA

Introduction

Patients surviving episodes of acute kidney injury (AKI) can recover their renal function without further consequences for many years. However, recent evidence based on epidemiological investigations and outcome analyses showed that AKI is a risk factor for the development and progression of chronic kidney disease (CKD), and, in particular, for promoting the transition of CKD to end-stage renal disease (ESRD) ultimately requiring dialysis.[1–3] AKI and CKD have been seen as an integrated clinical syndrome.[4] Hypoxia, inflammation,

microvascular rarefaction, and dysbiosis of gut microbiota have been linked to the AKI-to-CKD continuum.[2,5,6] Renal ischemia/reperfusion injury (IRI) has been used widely to investigate renal fibrosis from AKI to progressive CKD.[7–10] Renal fibrosis is always the common ultimate result of CKD, which is characterized by the process of epithelial-to-mesenchymal transition (EMT) and excessive accumulation and deposition of extracellular matrix (ECM) components.[11] Renal fibrosis is induced by the activation of a large number of growth factors, cytokines, chemokines and toxins, among which transforming growth factor-β1 (TGF-β1) and β-catenin are the central mediators in renal fibrosis.[12,13]

The TGF-β/Smad and Wnt/β-catenin pathways play a significant role in fibrogenesis of the kidney. TGF-β signaling is a central mediator in renal fibrosis of progressive CKD.[11,14] TGF-β exerts its profibrotic effect by transforming growth factor-β receptor II (TGFβRII), transforming growth factor-β receptor I (TGFβRI), and its intracellular mediators Smads. The combination of TGF-β1 and TGFβRII recruits and phosphorylates TGFβRI, which causes phosphorylation of Smad2 and Smad3 *via* the junction of adaptor proteins such as Smad anchor for receptor activation (SARA).[15] The phosphorylations of Smad2 and Smad3 regulate downstream profibrotic factor expressions. Smad4 also contributes to TGF-β1-induced fibrogenesis,[16] while Smad7 is a negative regulator of the TGF-β/Smad pathway by inhibition of Smad2 and Smad3 phosphorylation.[17] In the normal situation, the Wnt/β-catenin pathway is silent in adult kidney; once an injury occurs, Wnt/β-catenin signaling is reactive.[12,15] Sustained activation of the Wnt/β-catenin pathway plays a decisive role in driving the AKI-to-CKD continuum and accelerates renal fibrosis.[7] Profibrotic and fibrotic genes, including snail1, twist, plasminogen activator inhibitor-1 (PAI-1), fibroblast-specific protein 1 (Fsp-1) and matrix metalloproteinase-7 (MMP-7), are the downstream targets of Wnt/β-catenin signaling.[18] Since renin-angiotensin system (RAS) components are also directly downstream of Wnt/β-catenin signaling, the activation of Wnt/β-catenin signaling could upregulate the expression of RAS components to accelerate kidney injury.[19] Hence, inhibition of the TGF-β/Smad and Wnt/β-catenin pathways plays a critical role in attenuating renal fibrosis.

Although the molecular mechanisms underlying the AKI-to-CKD continuum have been partly revealed, no intervention has proved very effective to block the AKI-to-CKD continuum. Pharmacologic treatment to block the AKI-to-CKD continuum is urgently needed. In recent years, natural products have shown renoprotective and antifibrotic effects.[20–24] The surface layer of *Poria Cocos* (SLPC) exerts renoprotective effects,[25–29] and also has antifibrotic effects *via* regulation of the TGF-β/Smad and Wnt/β-catenin pathways.[30,31] Poricoic acid A (PAA), as a main triterpenoid compound of SLPC,[32] exhibits a good antifibrotic effect *in vivo* and *in vitro*. Additionally, melatonin, a secretory product of the pineal gland, has been reported to have antifibrotic effect in the kidney.[33–35] Although melatonin and PAA significantly alleviate renal fibrosis, their underlying mechanism remains undefined. In this study, we reveal the molecular mechanism of a combined melatonin and PAA intervention on the AKI-to-CKD continuum in renal IRI rats and hypoxia/reoxygenation (H/R) or TGF-β1 induced epithelial cells. Elucidating the molecular mechanism of the inhibitory effect of melatonin and PAA treatment on the AKI-to-CKD continuum will support the development of therapeutic options to prevent progression from AKI to CKD.

Materials and methods

Materials

Melatonin was purchased from Sigma-Aldrich (M5250, St. Louis, MO, USA). DMEM/F-12 and fetal bovine serum were purchased from Thermo Fisher Scientific (New York, NY, USA). SLPC was purchased from Shaanxi Medicinal Materials Company (Xi'an, Shaanxi, China). The primary antibodies were purchased from Abcam (Cambridge, MA, USA), Millipore (Billerica, MA, USA), CST (Danvers, MA, USA), BD Transduction Laboratories (San Jose, CA, USA), Santa Cruz (Dallas, TX, USA), and Proteintech (Wuhan, Hubei, China).

Primary antibodies against collagen I (ab34710, Abcam), alpha smooth muscle actin (α-SMA, ab7817, Abcam), fibronectin (ab2413, Abcam), vimentin (ab92547, Abcam), E-cadherin (ab76055, Abcam), Wnt1 (ab85060, Abcam), dephosphorylated active β-catenin (05-665,

Millipore), phosphorylated active β-catenin (Ser33/37/Thr41) (9561, CST), β-catenin (610154, BD Transduction Laboratories), snail1 (ab180714, Abcam), twist (ab50581, Abcam), MMP-7 (ab5706, Abcam), PAI-1 (612024, BD Transduction Laboratories), TGF-β1 (ab92486, Abcam), TGFβRI (ab31013, Abcam), SARA (ab124875, Abcam), p-Smad2 (3180, CST), Smad2 (5339, CST), p-Smad3 (9520, CST), Smad3 (9523, CST), Smad4 (38454, CST), Smad7 (sc-365846, Santa Cruz), p-ERK1/2 (4370, CST), ERK1/2 (9102, CST), p-p38 (4511, CST), p38 (8690, CST), p-PI3K (ab182651, Abcam), PI3K (4257, CST), α-tubulin (11224-1-AP, Proteintech), and β-actin (20536-1-AP, Proteintech) were used in the present study. The secondary antibodies goat anti-rabbit (A21000) and goat anti-mouse (A21010) were purchased from Abbkine (California, CA, USA).

Extraction and isolation of PAA

SLPC (20 kg) was powdered and extracted with 95% EtOH (100 l) three times. The solvent was removed under reduced pressure and crude extracts were obtained. The crude extracts (830 g) was subsequently dissolved in water and successively partitioned with petroleum ether, EtOAC, and *n*-BuOH to yield three fractions. EtOAC fractionation (500 g) was performed on MCI gel CHP20P, eluted with a gradient system of MeOH-H_2O (from 50:50 to 100:0) and yielded five fractions, A–F. Fraction C (60 g) was subjected to normal-phase fractionation on silica gel column chromatography using CH_2Cl_2-MeOH (from 100:1 to 1:1) and yielded seven fractions, C1–C7. Fraction C4 (12.1 g) was purified over RP-18 column chromatography using MeOH-H_2O elution system (from 50:50 to 100:0) and yielded fractions C41–C43. C42 (6.0 g) was then purified by reverse-phase semipreparative HPLC applying a MeOH-H_2O (85:15) elution system and a flow rate of 3 ml/min for 25 min.

Animals and treatment

All protocols concerning the use of animals were carried out in accordance with the recommendations in the Guide for the Care and Use of Laboratory Animals of the State Committee of Science and Technology of the People's Republic of China, and were approved by the Committee on the Ethics of Animal Experiments of the Northwest University (Permit Number: SYXK2010-004). Male Sprague-Dawley rats with an age of 7 weeks old, weighing 180–200 g, were purchased from the Central Animal Breeding House of Fourth Military Medical University (Xi'an, Shaanxi, China). Rats were provided with food and water *ad libitum*, and housed in plastic cages (four rats per cage) placed in a normal conditioned vivarium with 40–70% humidity at 22 ± 2°C and 12 h light/12 h dark cycle. Rats were acclimated to their housing environment for 7 days prior to experimentation, and to the experimental room for 1 h before experiments. Animal studies are reported in compliance with ARRIVE guidelines. Rats were divided randomly into five groups (n = 7 each): (1) sham, (2) IRI, (3) IRI + melatonin, (4) IRI + PAA, and (5) IRI + melatonin + PAA group. After being anesthetized with chloral hydrate by intraperitoneal injection (10%, 10 ml/kg), IRI rats were induced by clamping the bilateral renal pedicles for 1 h using a nontraumatic bulldog clamp. Sham rats received laparotomy only. After reperfusion, rats were given melatonin at a dose of 20 mg/kg by intraperitoneal injection at 30 min and 50 mg/kg at 6 h and 18 h. In addition, melatonin (50 mg/kg) was given by intraperitoneal injection from day 1 to day 7 after reperfusion in the morning. PAA (10 mg/kg) was given by gavage from day 1 to day 14 after reperfusion in the morning. Under general anaesthesia, all rats were sacrificed at the end of the 2nd week in the morning. The ligated kidneys were separated into two parts. One was immediately frozen and saved in liquid nitrogen for western blot and qRT-PCR analyses, and the other was used for immumohistochemical staining to investigate the therapeutic effects of melatonin and PAA against renal fibrosis.

Cell culture and treatment

HK-2 cells were cultured in DMEM-F12 supplemented with 10% fetal bovine serum with 5% CO_2 at 37°C. HK-2 cells were divided into seven groups (n = 5): control (CTL), melatonin (MEL), PAA, H/R, H/R + melatonin (H/R + MEL), H/R + PAA, and H/R + melatonin + PAA (H/R + MEL + PAA). H/R cells were placed in a hypoxic chamber under 0% O_2 atmosphere for 6 h, and then placed under normal conditions for reoxygenation for 12 h. During reoxygenation, the treated groups were incubated

with melatonin (10 μM) and PAA (10 μM). Additonally, TGF-β (2.5 ng/ml) was also used to stimulate HK-2 cells

Lentivirus expressing full-length human Wnt1 cDNA (Wnt1 over) was constructed by Sangon (Shanghai, China). Lipofectamine 3000 was used according to the manufacturer's guide.

Knockdown of Smad3 by small interfering RNA

Specific Smad3 small interfering RNA (siRNA) (5'-CCGCAUGAGCUUCGUCAAATT-3') or control siRNA (CTL siRNA) (5'-UUCUCCG AACGUGUCACGUTT-3') was synthesized by Sangon (Guangzhou, Guangdong, China). HK-2 cells were cultured in six-well plates and transfected with 3 μl of 10 μM siRNA/well by using 9 μl lipofectamine RNAiMAX (Invitrogen, New York, NY, USA). After incubation for 48 h, the HK-2 cells were used for subsequent experiments.

Histology and immunohistochemical staining

Kidney tissues were fixed in 4% paraformaldehyde overnight, subsequently processed for paraffin embedding, then sectioned at 5 μm. Kidney sections were deparaffinized and hydrated through a graded ethanol series, then stained with periodic acid–Schiff (PAS) reagent using a standard protocol.[19] Immunohistochemical staining was performed using a routine protocol.[36]

Immunofluorescence staining and confocal microscopy

HK-2 cells were cultured on coverslips and fixed with 4% paraformaldehyde for 10 min. After blocking with 10% goat serum for 30 min, the cells were immunostained with primary antibodies at 4°C overnight. After washing three times with PBS, cells were incubated with the corresponding secondary antibodies for 2 h at room temperature. The cells were mounted with 80% glycerinum in PBS and subsequently examined by a laser-scanning confocal microscope (FV1000, Olympus Corporation, Tokyo, Japan) equipped with FV10-ASW 4.0 VIEW.

Protein extraction and Western blotting analysis

Kidney tissues and cells were lysed in RIPA buffer and protein concentrations were measured with a Pierce™ BCA Protein Assay Kit (23227, Thermo Scientific, New York, NY, USA). Standard western blots were performed. Briefly, 20–30 μg of protein was separated by 8–12% SDS-PAGE gel and transferred to PVDF membranes. After blocking in 5% nonfat milk buffer, blots were probed with primary antibodies. After incubation with corresponding secondary antibodies, immunoblots were visualized by Amersham ECL prime western blotting detection reagent (RPN2232, GE Healthcare, New York, NY, USA). Signal intensities were quantified with ImageJ software (version 1.48 v, NIH, Bethesda, MD, USA). α-Tubulin or β-actin was used as a loading control. Quantification of each protein was repeated three times.

Quantitative real-time PCR

Total mRNA was extracted with Trizol reagent (Invitrogen). The mRNA (0.5 μg) was used to synthesize cDNA using a Transcriptor First Strand cDNA Synthesis Kit (Roche, Mannheim, Germany). Quantitative real-time PCR (qRT-PCR) was conducted using SYBR® Premix Ex Taq™ II (Takara Bio, Otsu, Shiga, Japan). The primer sequences are listed in Table 1. Samples were amplified for 40 cycles using a Bio-Rad CFX 96 Touch™ system (Bio-Rad, Hercules, CA, USA). mRNA levels, normalized to GAPDH (human) or β-actin (rat), were determined using the comparative ΔΔCt method.[12]

Coimmunoprecipitation

The interactions of Smad2 or Smad3 with TGFβRI and SARA were determined by coimmunoprecipitation (Co-IP). After pretreatment with protein A/G (Immunoprecipitation Starter Pack, GE Healthcare, NY, New York, USA) for 1 h at 4°C to remove antibodies present in lysates, supernatants were transferred into a fresh Eppendorf tube. The supernatants were incubated with anti-TGFβRI (1:50) or SARA antibody (1:50) overnight at 4°C to couple antigen to antibody, and then immunoprecipitated by protein A/G to precipitate the immune complexes. After washing three times with lysis buffer, the supernatants were boiled for 3 min in sample buffer.

To investigate the interaction of Smad3 and β-catenin in the nucleus, nucleoprotein was extracted using NE-PER Nuclear and Cytoplasmic Extraction Reagents (78835, Thermo Scientific,

Table 1. Nucleotide sequences of the primers used for qRT-PCR.

Gene	Forward	Reverse	Product size (bp)
Rat			
Wnt1	CATCGTGAACATAGCCTCCTC	ATCAGTCGTCGCTGCTTG	108
Wnt2	GCCTTTGTTTACGCCATCTC	GATCGCAGGAACAGGACTTTA	91
Wnt3	GCAAATGCCATGGGTTGTC	CGTACTTGTCCTTGAGGAAGTC	99
Wnt3a	TGCAAATGCCACGGACTAT	GGTGTTTCTCTACCACCATCTC	133
Wnt7a	GATCCTGGAGGAGAACATGAAA	GTAGCCTAGCTCTCGGAATTG	109
Wnt8a	CATGTACGCTGTCACCAAGA	CCACCTGCTTTCCCATTATTTG	84
β-actin	GTGCCCATCTATGAGGGTTATG	GCTGTGGTCACGAAGGAATAG	125
Human			
Wnt1	CTGGCTGGGTTTCTGCTAC	GAGGAGGCTACGTTCACAATAC	106
Wnt2	CTCCTCAGCTGGAGTTGTATTT	GGCGCTTCCCATCTTCTT	94
Wnt3	GGCTGTGACTCGCATCATAA	GAACTCCCTGGACACTAACAC	99
Wnt3a	TGTTGGGCCACAGTATTCC	GGCATGATCTCCACGTAGTT	111
Wnt7a	CGTTCACCTACGCCATCATT	GTACTGGCCTTGCTTCTCTTT	110
Wnt8a	CAGTGAGAGCCACCATGAAA	CCTGGTCATACTTGGCCTTTAG	132
GAPDH	GGTGTGAACCATGAGAAGTATGA	GAGTCCTTCCACGATACCAAAG	123

New York, NY, USA), using anti-β-catenin antibody (1:100).

Chromatin immunoprecipitation assay

β-Catenin protein complex binding to chromosomal DNA was evaluated in rats and HK-2 cells by chromatin immunoprecipitation (ChIP) assay. The ChIP assay was carried out using a Pierce Agarose ChIP Kit (26156, New York, NY, USA) according to the manufacturer's instructions. DNA/protein complexes were crosslinked for 10 min in formaldehyde (28906, New York, NY, USA) at a final concentration of 1%. The fixed kidney tissues or cells were lysed to obtain nuclei. Chromatin was digested by employing micrococcal nuclease at 4°C for 5 min. For immunoprecipitation, cell lysates were incubated with an antibody against β-catenin (3 μg) and incubated overnight at 4°C on a rocking platform, while immunoprecipitation with normal rabbit IgG was used as a control. The immunoprecipitations were subjected to qRT-PCR with primer sets that amplify angiotensinogen (AGT), renin, angiotensin-converting enzyme (ACE), angiotensin II type 1 receptor (AT1R), snail1, twist, PAI-1, and MMP–7. Primers for ChIP were designed and synthesized by Sangon (Guangzhou, Guangdong, China). The primer sequences are listed in Table 2. Fold-enrichment relative to the IgG antibody control (negative control) set to 1.0 was calculated using the comparative CT method (ΔΔCt).

Smad3-dependent promoter assay

HK-2 cells were transfected with the Smad3-responsive promoter p(GAGA)12-luc as previously described.[37] Lipofectamine 3000 (Invitrogen, New York, NY, USA) was employed to perform the transfection according to the manufacturer's instructions. After transfection, HK-2 cells were treated as indicated. Luciferase activity was analyzed by a luciferase reporter gene assay kit (Roche, Mannheim, Germany) according to the manufacturer's instructions, and normalized by protein concentration.

Table 2. Nucleotide sequences of the primers used for ChIP.

Gene	Forward	Reverse	Product size (bp)
Rat			
Snail	CGCTACCGTAGATGGGAATTAG	ACTTCATTACTGCTGGGTGTAG	130
Twist	ACCTCTTTGAAGCTCTTGGG	GGAGATCGCGTGAGTAGTTATG	109
MMP-7	TCTCTCTCTCTCTCTCTCTCT	GCGAGAGGCCTTAGTTTCTATT	100
PAI-1	CAAGGTGCAGGTCTTGAATTG	CTCCTCTCCCTTCTTCCTTCTA	102
Human			
AGT	CAGGCTGTGACAGGATGGAA	GCTGTTGTCCACCCAGAACT	150
Renin	TTGTGGGCATGGGCTTCATT	CAATCTGTCCTCCCAGCGAT	150
ACE	CCAACCTGCCCCTGGCTAAG	GCGAGGAAGCCAGGATGTT	150
AT1R	GGAAACAGCTTGGTGGTGAT	CCAGCGGTATTCCATAGCTG	150

Statistics

Data are described as means ± SD. Comparison between groups were assessed by one-way ANOVA by *post hoc* test using GraphPad Prism software v 5.0 (GraphPad Software, San Diego, CA, USA). $p < 0.05$ was considered to be statistically significant.

Results

Melatonin and PAA attenuate IRI-induced renal fibrosis and retard the AKI-to-CKD continuum

As shown in Figure 1(a, b), compared with sham rats, significant upregulation of α-SMA, collagen I and fibronectin expression pointed to marked interstitial fibrosis in IRI rats at day 14 after the IRI procedure. Following treatment with melatonin and PAA, alpha smooth muscle actin (α-SMA) collagen I and fibronectin were reduced (compared with IRI rats, $p < 0.05$). Both melatonin and PAA showed inhibitory effects, while the combination of melatonin and PAA performed better than either used alone ($p < 0.05$). Since TGF-β1 plays a central role in fibrogenesis, we measured the mRNA and protein expression of TGF-β1. As shown in Figure 1(c–e), renal IRI resulted in the upregulation of TGF-β1 at both mRNA and protein levels (compared with sham rats, $p < 0.05$) from AKI to CKD, while melatonin and PAA suppressed aberrant TGF-β1 expression. Notably, combined therapy showed a stronger inhibitory effect than either compound used alone during the AKI-to-CKD continuum ($p < 0.05$).

Melatonin inhibits TGF-β1 pathway while PAA selectively suppresses p-Smad3 in renal IRI rats

In general, TGF-β1 exerts its profibrotic effect through Smad-dependent and Smad-independent pathways, which include p38, ERK1/2, and PI3K.[14] To gain a comprehensive understanding of underlying mechanisms of melatonin and PAA, we examined the status of both Smad-dependent and Smad-independent pathways in IRI rats. As shown in Figure 2(a, b), compared with sham rats, IRI induced significant upregulation of p-Smad2, Smad2, p-Smad3, Smad3, and Smad4, and downregulation of Smad7 ($p < 0.05$), and treatment with melatonin prevented this aberrant upregulation ($p < 0.05$). However, treatment with PAA selectively inhibited p-Smad3 upregulation ($p < 0.05$), which indicated different mechanisms of melatonin and PAA. Of note, PAA showed a stronger inhibitory effect on p-Smad3 than melatonin ($p < 0.05$). As shown in Figure 2(c, d), upregulation of p-Smad2 and p-Smad3 in the nucleus decreased markedly after melatonin and PAA intervention at day 14 after the IRI procedure (compared with IRI rats, $p < 0.05$), which is consistent with western blotting results. Although PAA hardly affected p-Smad2 expression, PAA could enhance the inhibitory effect of melatonin to decrease the

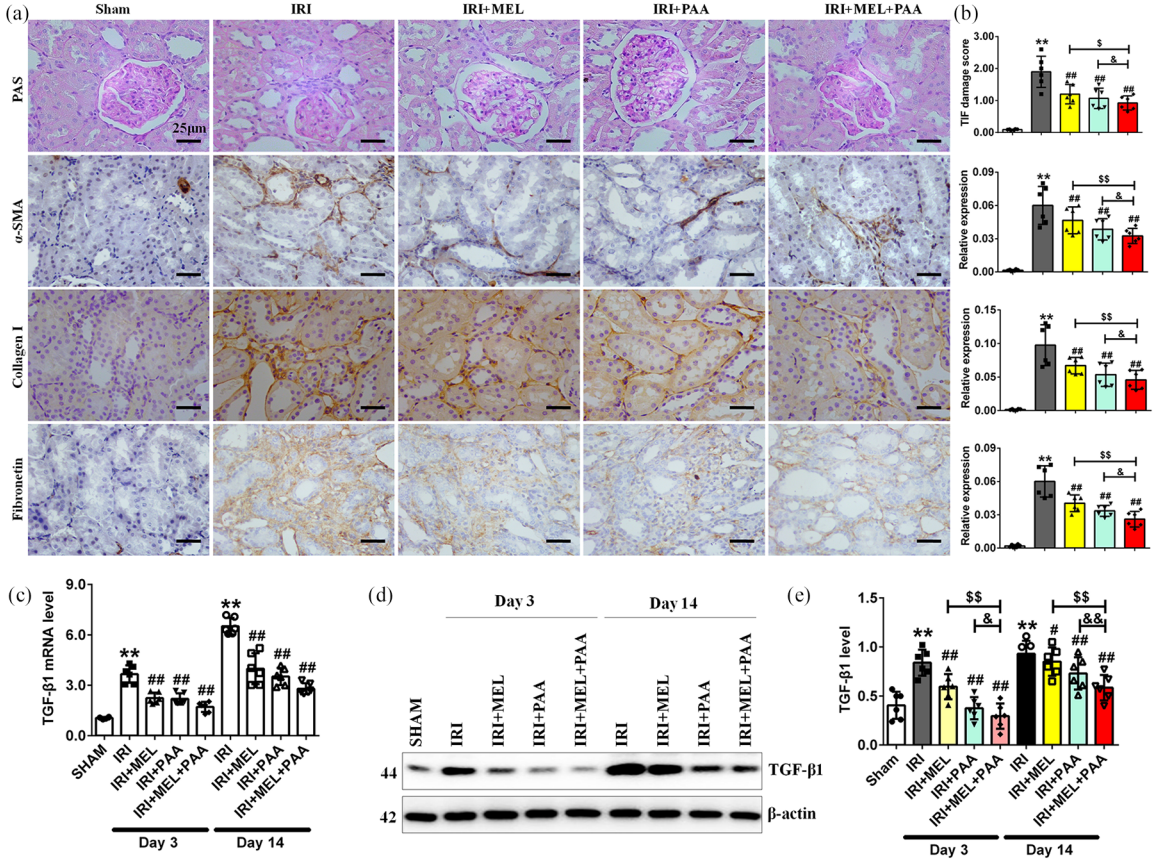

Figure 1. The renoprotective and anti-fibrotic effects of melatonin and PAA. (a, b) Representative micrographs of PAS staining, α-SMA, collagen I, and fibronectin protein expression in indicated groups at day 14 after the IRI procedure. Scale bar, 25 μm. (c) mRNA level of TGF-β1 in indicated groups. (d, e) Protein level of TGF-β1 in indicated groups. Data represented as mean ± SD ($n = 7$).

IRI, Ischemia-reperfusion injury; PAA, poricoic acid A; PAS, periodic acid–Schiff; α-SMA, alpha smooth muscle actin; TGF-β1, transforming growth factor-β1.

$^{**}p < 0.01$ *versus* sham group; $^{\#\#}p < 0.01$ *versus* IRI group; $^{\$}p < 0.05$; $^{\$\$}p < 0.01$ *versus* IRI + melatonin group; $^{\&}p < 0.05$; $^{\&\&}p < 0.01$ *versus* IRI + PAA group.

expression of p-Smad2 and p-Smad3, indicating that supplementation with PAA enhanced the inhibitory effects of melatonin.

The Smad-independent pathway was further explored. We examined the expression of p-ERK1/2, ERK1/2, p-PI3K, PI3K, p-p38, and p38, which promoted fibrogenesis.[14,38] As shown in Figure 2(e, f), compared with sham rats, increased levels of p-ERK1/2, ERK1/2, p-PI3K, PI3K, p-p38, and p38 were detected in IRI rats ($p < 0.05$). The upregulation of p-ERK1/2, ERK1/2, p-PI3K, PI3K, p-p38, and p38 in the kidney of IRI rats was significantly inhibited by melatonin treatment, while PAA barely reversed these abnormalities, indicating entirely different mechanisms of melatonin and PAA. Taken together, the results indicate that melatonin exerted an extensive inhibitory effect on the downstream mediators of TGF-β1, while PAA selectively suppressed the upregulation of p-Smad3.

Melatonin ameliorated H/R-induced activation of the TGF-β1 pathway while PAA attenuated only p-Smad3 expression

To further investigate the underlying mechanism of melatonin and PAA *in vitro*, H/R-induced HK-2 cells were employed. As shown in Figure 3(a–c), compared with the CTL group, upregulation of TGF-β1, p-Smad2, p-Smad3, and Smad4, and downregulation of Smad7, was observed after H/R stimulation ($p < 0.05$), indicating activation of the TGF-β1/Smad pathway. Treatment

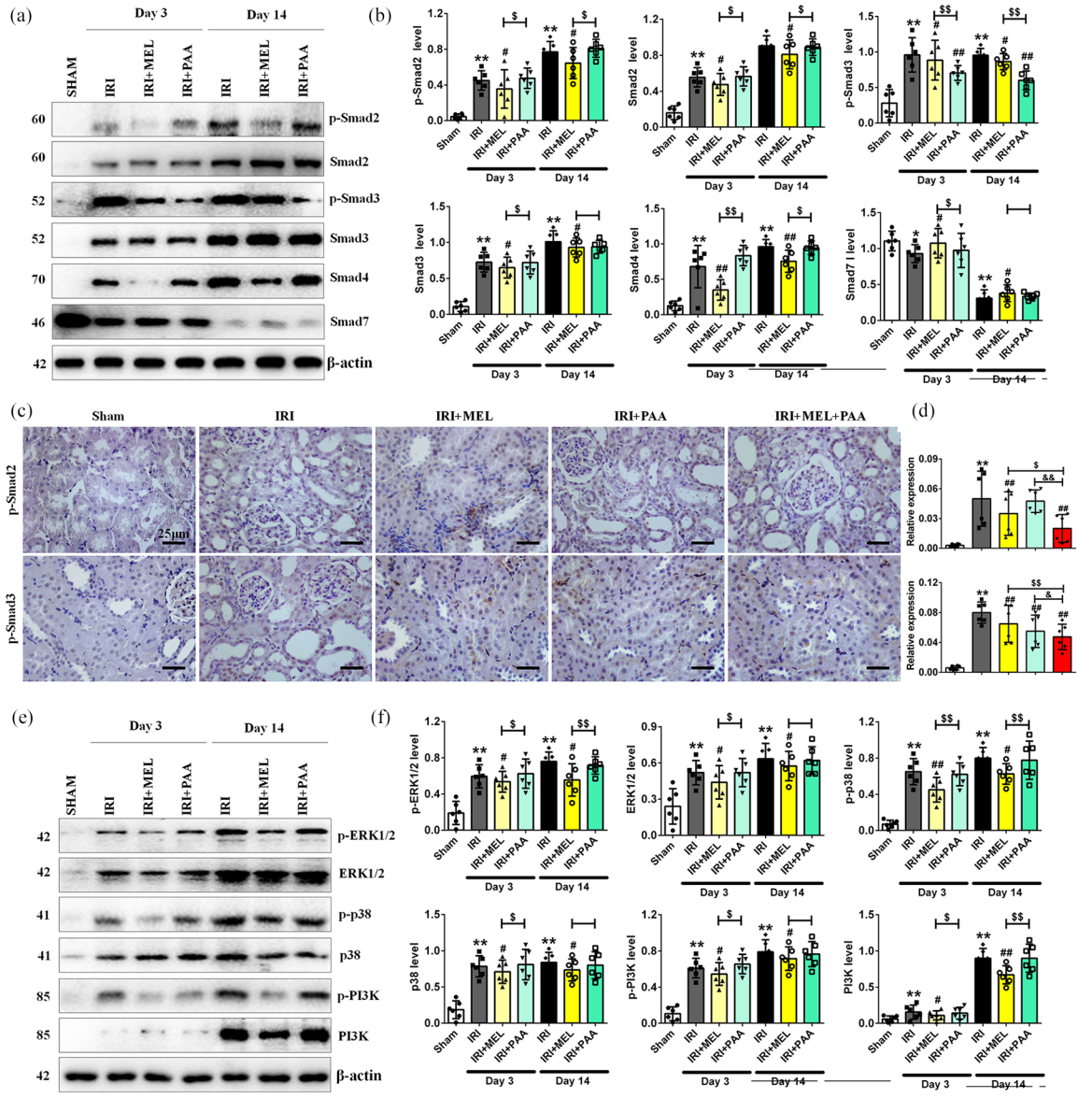

Figure 2. Inhibitory effects of melatonin and PAA against activation of the Smad-dependent and Smad-independent pathways *in vivo*. (a, b) Protein levels of p-Smad2, Smad2, p-Smad3, Smad3, Smad4, and Smad7 in indicated groups. (c, d) Representative micrographs of p-Smad2 and p-Smad3 protein expression in indicated groups. Scale bar, 25 μm. (e, f) Protein levels of p-ERK1/2, ERK1/2, p-p38, p38, p-PI3K and PI3K in indicated groups. Data represented as mean ± SD ($n = 7$).
PAA, poricoic acid A.
$^{**}p < 0.01$ *versus* sham group; $^{\#}p < 0.05$; $^{\#\#}p < 0.01$ *versus* IRI group; $^{\$}p < 0.05$; $^{\$\$}p < 0.01$ *versus* IRI + melatonin group; $^{\&}p < 0.05$; $^{\&\&}p < 0.01$ *versus* IRI + PAA group.

with melatonin significantly inhibited the upregulation of p-Smad2, p-Smad3, and Smad4, and increased Smad7 expression (compared with the H/R group, $p < 0.05$). Treatment with PAA suppressed only the upregulation of p-Smad3 (compared with the H/R group, $p < 0.05$), which was consistent with the results of IRI rats. As shown in Figure 3(c, d), immunofluorescence staining indicated that H/R induced p-Smad3 nuclear translocation, while melatonin and PAA attenuated this effect in HK-2 cells. Notably, PAA exerted a better inhibitory effect than melatonin

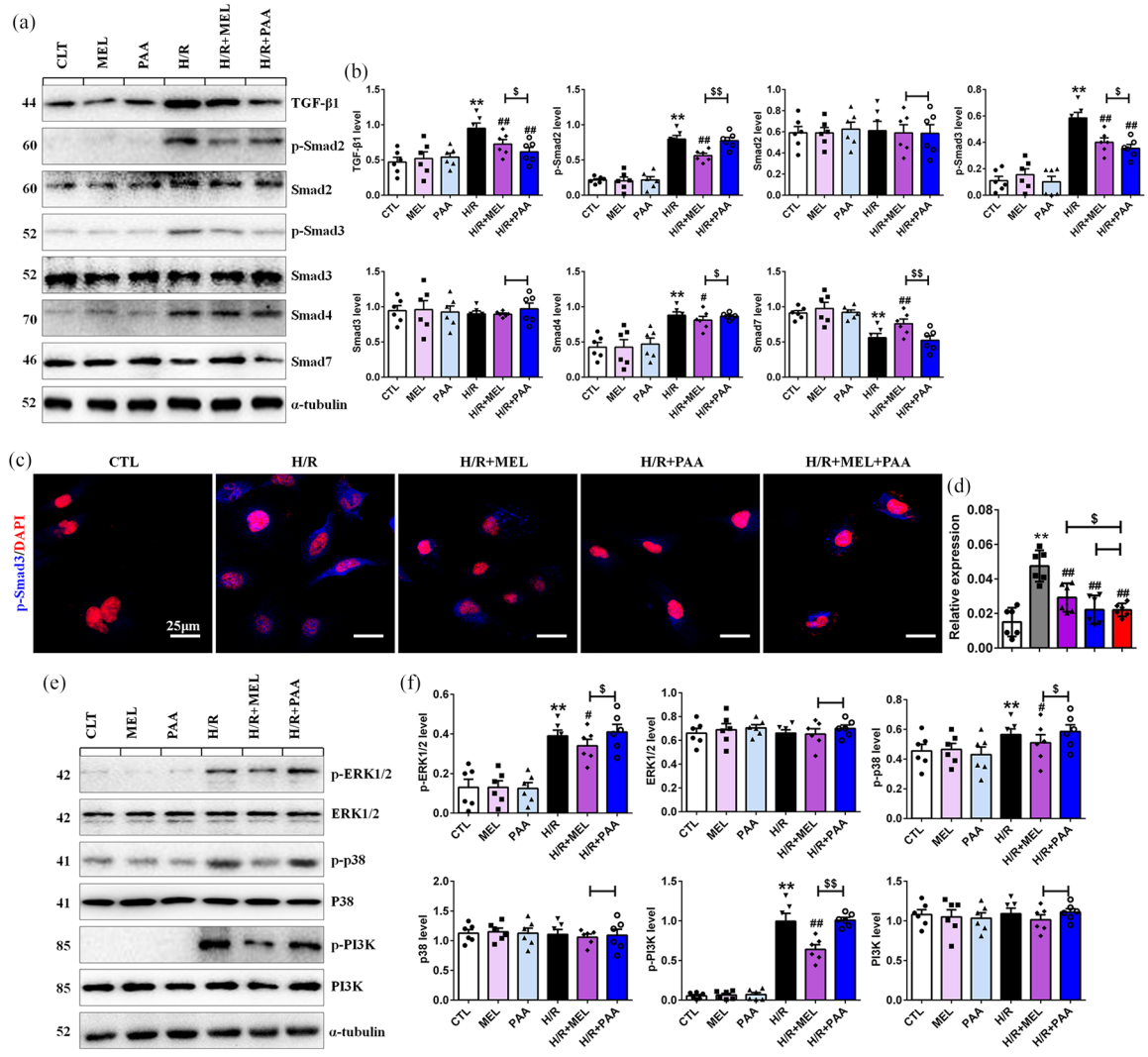

Figure 3. The inhibition of melatonin and PAA against the activation of Smad-dependent and Smad-independent pathways *in vivo*. (a, b) Protein levels of TGF-β1, p-Smad2, Smad2, p-Smad3, Smad3, Smad4, and Smad7 in indicated groups in HK-2 cells. (c, d) Immunofluorescence staining of p-Smad3 (blue) in indicated groups. Scale bar, 25 μm. (e, f) Protein levels of p-ERK1/2, ERK1/2, p-p38, p38, p-PI3K, and PI3K in indicated groups. Data represented as mean ± SD ($n = 6$).
H/R, hypoxia/reoxygenation; PAA, poricoic acid A.
$^{**}p < 0.01$ *versus* CTL group; $^{\#}p < 0.05$; $^{\#\#}p < 0.01$ *versus* H/R group; $^{\$}p < 0.05$; $^{\$\$}p < 0.01$ *versus* H/R + melatonin group.

on Smad3 nuclear translocation ($p < 0.05$), and the combined therapy performed better than either compound alone (compared with H/R + melatonin or H/R + PAA group, $p < 0.05$). To further confirm the renoprotective role of melatonin and PAA, TGF-β1 was used to stimulate HK-2 cell. As shown in Figure S1, TGF-β1 triggered the upregulation of Smad3, but treatment with melatonin or PAA significantly inhibited this abnormality (compared with H/R group, $p < 0.05$). As shown in Figure 3(e, f), H/R resulted in the upregulation of p-ERK1/2, p-p38, and p-PI3K in HK-2 cells (compared with CTL group, $p < 0.05$). Melatonin treatment markedly suppressed the upregulation of p-ERK1/2, p-p38, and p-PI3K, while PAA had no effect on these dysregulations (compared with H/R group, $p < 0.05$).

These results point to the conclusion that melatonin targets multiple downstream mediators of TGF-β1, while PAA selectively inhibits

phosphorylation of Smad3, indicating Smad3 as the main therapeutic target of PAA.

Smad3 is the main therapeutic target of PAA in renal fibrosis while melatonin has multiple targets

To further confirm our conclusion that Smad3 is the main therapeutic target of PAA, Co-IP and RNA interference (RNAi) was employed. As shown in Figure 4(a–d), the interactions of Smad2 or Smad3 with TGFβRI and SARA were observed in rats following the IRI procedure ($p < 0.05$). Treatment with melatonin weakened the interactions of Smad2/3 with TGFβRI and SARA in IRI rats (compared with IRI group, $p < 0.05$), while PAA selectively affected the interactions of Smad3 with TGFβRI and SARA. Of note, PAA showed a stronger inhibitory effect than melatonin on the interactions of Smad3 with TGFβRI and SARA, indicating that PAA exerted its antifibrotic effects mainly through inhibition of phosphorylation of Smad3. The luciferase reporter system containing the promoter region of the human collagen I gene was employed to detect activity of the Smad3 promoter. Melatonin and PAA largely mitigated H/R-induced Smad3-dependent collagen I promoter activity (Figure 4e).

RNAi was employed to further verify this conclusion. As shown in Figure 4(f, g), specific Smad3 siRNA significantly inhibited Smad3 protein expression ($p < 0.05$), and melatonin and PAA did not affect the process of RNAi. Smad3 siRNA also inhibited H/R-induced collagen I and α-SMA expression (Figure S2). As shown in Figure 4(h, i), after knockdown of Smad3, the protein expression of profibrotic vimentin, α-SMA, collagen I, and fibronectin were significantly increased in H/R + melatonin or H/R + PAA groups (compared with H/R group, $p < 0.05$). Since Smad3 was the therapeutic target of melatonin and PAA, the loss of the therapeutic target resulted in partially weakened antifibrotic effects, especially PAA. Notably, after knockdown of Smad3, fibronectin protein expression was barely reversed after PAA treatment (compared with H/R group, $p > 0.05$). The same results were also observed under TGF-β1 stimulation (Figure S3). These data support the view that Smad3 serves as the main therapeutic target of PAA, and the loss of Smad3 partly weakens the antifibrotic effects of PAA and melatonin.

PAA and melatonin inhibit the Wnt/β-catenin pathway and profibrotic target genes in renal IRI rats

Wnt/β-catenin plays a vital role in the occurrence and development of renal disease, especially renal fibrosis. We first investigated the mRNA expression of several Wnt genes in IRI rats. As shown in Figure 5(a, b), a comprehensive survey of Wnt genes revealed that several Wnts, including Wnt1, Wnt2, Wnt3, Wnt3a, Wnt7a, and Wnt8a, were markedly upregulated at 3 and 14 days in IRI rats (compared with sham rats, $p < 0.05$). As shown in Figure 5(c, d), immunohistochemical stainings demonstrated that IRI caused the upregulation of Wnt1 and β-catenin in renal tubules at day 14 after the IRI procedure ($p < 0.05$). Both melatonin and PAA treatment significantly improved the upregulation of Wnt1 and β-catenin, while combined therapy showed a stronger inhibitory effect (compared with IRI + melatonin or IRI + PAA group, $p < 0.05$). Figure 5(e, f) shows the increases of Wnt1, active β-catenin, and β-catenin, and the decrease of nonactive p-β-catenin, which indicates activation of the Wnt/β-catenin pathway in IRI rats (compared with sham rats, $p < 0.05$). The inhibitory effect of PAA was stronger than that of melatonin on these dysregulations (compared with IRI + melatonin group, $p < 0.05$). Next, we examined downstream targets of the Wnt/β-catenin pathway. As shown in Figure 5(g, h), the upregulation of snail1, twist, PAI-1, and MMP-7 was detected in IRI rats (compared with sham rats, $p < 0.05$). Both melatonin and PAA treatment significantly attenuated these dysregulations, while treatment with PAA performed better than melatonin (compared with IRI + melatonin group, $p < 0.05$). We further verified these results by ChIP assay. As shown in Figure 5I, J, IRI activated the β-catenin-mediated transcription of snail1, twist, PAI-1, and MMP-7 at 3 and 14 days in IRI rats (compared with sham rats, $p < 0.05$). Treatment with melatonin and PAA significantly reduced the upregulation of transcription, while combined therapy showed stronger inhibitory effects than each compound used alone (compared with IRI + melatonin or IRI + PAA group, $p < 0.05$). Additionally, the inhibitory effects of PAA were stronger than those of melatonin (compared with IRI + melatonin group, $p < 0.05$). Taken together, melatonin and PAA treatment simultaneously

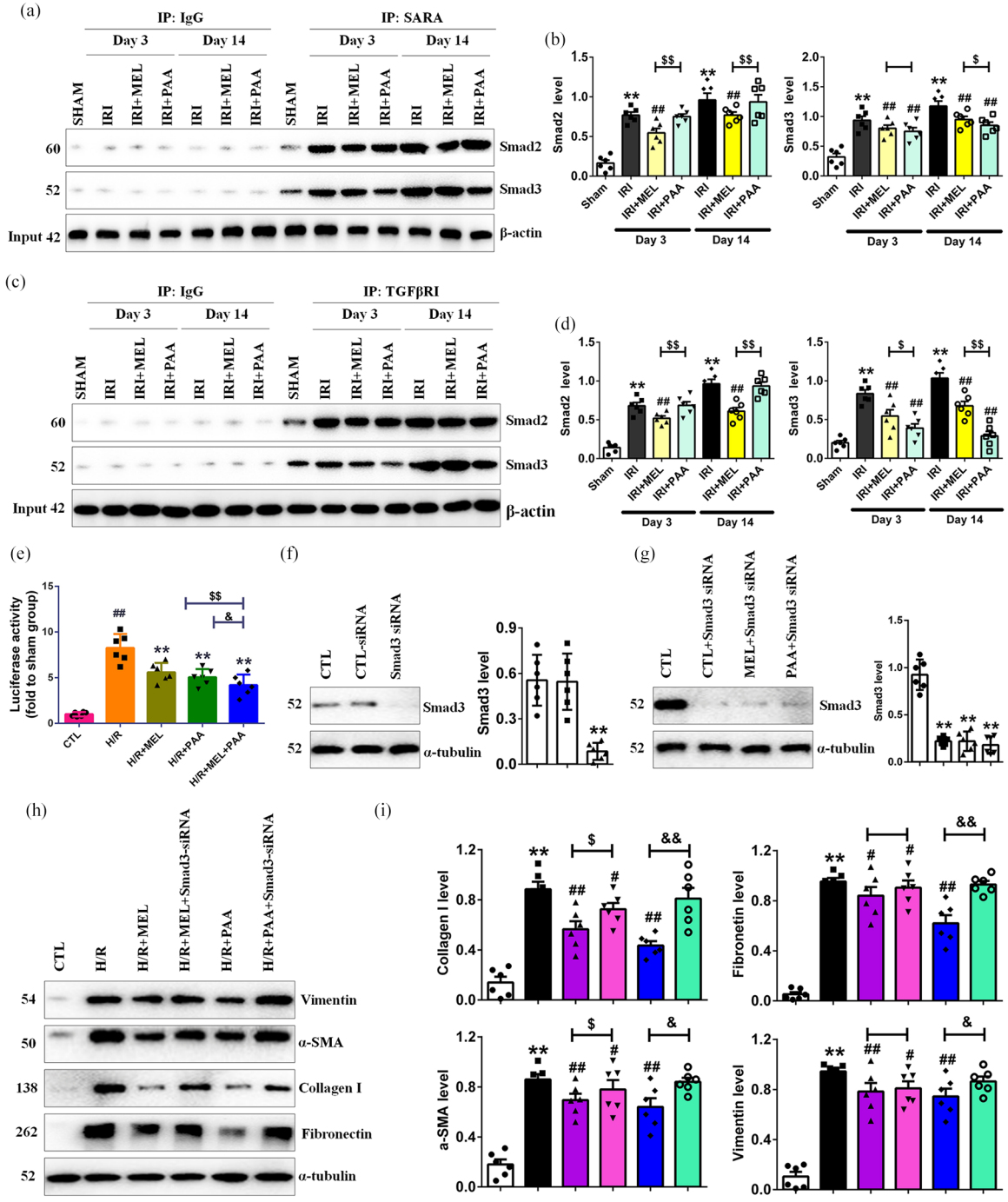

Figure 4. Interference effects of melatonin and PAA on Smad2/3 phosphorylation. (a, b) Co-IP bands of Smad2 and Smad3 in indicated groups. (c, d) Co-IP bands of Smad2 and Smad3 in indicated groups. (e) Luciferase activity in indicated groups after cotransfected with p(CACA)-luciferase plasmid and PGL3. (f) Protein level of Smad3 in indicated groups. (g) Protein level of Smad3 in indicated groups. (h, i) Protein levels of vimentin, α-SMA, collagen I, and fibronectin in indicated groups. Data represented as mean ± SD ($n = 6$).

Co-IP, Coimmunoprecipitation; PAA, poricoic acid A; α-SMA, alpha smooth muscle actin.

$^{**}p < 0.01$ *versus* CTL or sham group; $^{\#}p < 0.05$; $^{\#\#}p < 0.01$ *versus* H/R or IRI group; $^{\$}p < 0.05$; $^{\$\$}p < 0.01$ *versus* IRI + melatonin or H/R + melatonin group; $^{\&}p < 0.05$; $^{\&\&}p < 0.01$ *versus* H/R + PAA group.

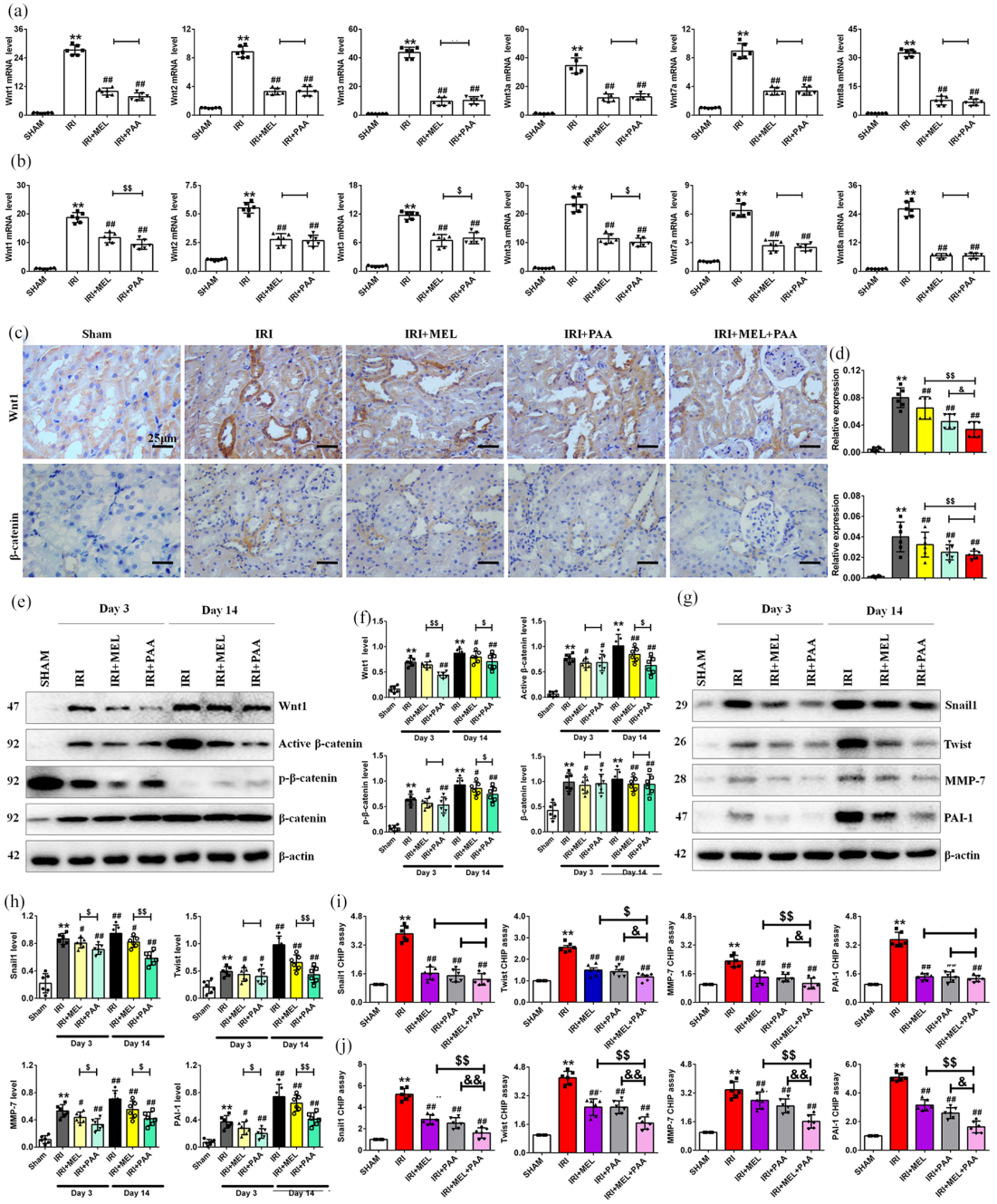

Figure 5. Inhibitory effect of melatonin and PAA on the activation of the Wnt/β-catenin pathway *in vivo*. (a) The mRNA levels of Wnt1, Wnt2, Wnt3, Wnt3a, Wnt7a, and Wnt8a in different groups (3 days after IRI procedure). (b) The mRNA levels of Wnt1, Wnt2, Wnt3, Wnt3a, Wnt7a, and Wnt8a in different groups (14 days after IRI procedure). (c, d) Representative micrographs of Wnt1 and β-catenin protein expression in indicated groups at day 14 after IRI procedure. Scale bar, 25 μm. (e, f) Protein levels of Wnt1, active β-catenin, p-β-catenin, and β-catenin in indicated groups. (g, h) Protein levels of snail1, twist, MMP-7, and PAI-1 in indicated groups. (i) ChIP assay results of snail1, twist, MMP-7, and PAI-1 in different groups (3 days after IRI procedure). (j) ChIP assay results of snail1, twist, MMP-7, and PAI-1 in different groups (14 days after IRI procedure). Data represented as mean ± SD ($n = 7$).

ChIP, chromatin immunoprecipitation; MMP-7, matrix metalloproteinase-7; PAA, poricoic acid A; PAI-1, plasminogen activator inhibitor-1.

$^{**}p < 0.01$ *versus* sham group; $^{\#}p < 0.05$; $^{\#\#}p < 0.01$ *versus* IRI group; $^{\$}p < 0.05$; $^{\$\$}p < 0.01$ versus IRI + melatonin group; $^{\&}p < 0.05$; $^{\&\&}p < 0.01$ *versus* IRI + PAA group.

retarded the activation of Wnt/β-catenin and downstream target expression, while PAA had a larger inhibitory effect than melatonin.

Combined therapy inhibits the Wnt/β-catenin pathway and mediates transcription of RAS components

To further confirm the inhibitory effects of melatonin and PAA treatment on the activation of Wnt/β-catenin signaling, H/R-induced HK-2 cells were employed. As shown in Figure 6(a), increases in Wnt1, Wnt2, Wnt3, Wnt3a, Wnt7a, and Wnt8a were detected after H/R stimulation (compared with CTL group, $p < 0.05$). Compared with the H/R group, melatonin and PAA treatment significantly mitigated this mRNAs dysregulation ($p < 0.05$). As shown in Figure 6(b–e), the upregulation of Wnt1, active β-catenin, snail1, twist, PAI-1, and MMP-7, and downregulation of p-β-catenin induced by H/R stimulation were significantly improved by melatonin and PAA treatment, and PAA had greater inhibitory effects than melatonin (compared with H/R + melatonin group, $p < 0.05$). Additionally, melatonin and PAA also inhibited activation of the Wnt/β-catenin pathway under conditions of Wnt1 overexpression (Figure S4), which further confirmed the inhibitory effects of melatonin and PAA against Wnt/β-catenin activity. RAS components are also downstream targets of the Wnt/β-catenin signaling that induces fibrosis.[19] We further examined β-catenin-mediated AGT, renin, ACE, and AT1R transcription. Compared with the CTL group, H/R stimulation increased β-catenin-mediated transcriptions of AGT, renin, ACE, and AT1R in HK-2 cells ($p < 0.05$). Both melatonin and PAA treatment inhibited the effects of β-catenin on the transcriptional activity of these genes, while combined therapy resulted in stronger inhibitory effects.

PAA exhibits stronger inhibitory effects than melatonin against the interaction of Wnt/β-catenin and TGF-β/Smad pathway

As shown in Figure 7(a, b), IRI induced the interaction of Smad2 and Smad3 with β-catenin at day 14 after the IRI procedure (compared with sham group, $p < 0.05$). Melatonin treatment disturbed the interaction of Smad2 and Smad3 with β-catenin, while PAA selectively inhibited the interaction of Smad3 with β-catenin. Notably, combined therapy exhibited stronger effects against the interaction of Smad2 and Smad3 with β-catenin. The same results were observed in H/R-induced HK-2 cells (Figure 7c, d). Inhibition of the interaction of Smad2 and Smad3 with β-catenin may be one of the reasons for the anti-fibrotic effects of melatonin and PAA.

Discussion

Ischemic kidney injury is the critical cause of AKI in hospitalized patients, and is related to high morbidity and mortality rates. Incomplete recovery from AKI is a well-recognized pathway to progressive CKD.[2] AKI can cause CKD directly, and increase the risk of developing incident ESRD. Renal IRI is the common cause that triggers the AKI-to-CKD continuum. Knowledge of the molecular mechanisms of the AKI-to-CKD continuum has been partly revealed,[2] but few pharmacological approaches effectively prevent it. AKI induces impairments in tubular cells that generate massive production of profibrotic cytokines, including TGF-β1 and β-catenin, and these mediators result in the EMT and excessive ECM production that eventually causes renal fibrosis.[1] Among profibrotic cytokines, TGF-β1 plays a central role in fibrogenesis. Additionally, the persistent activation of Wnt/β-catenin signaling promotes AKI to progressive CKD.[7] Hence, the inhibition of TGF-β and Wnt/β-catenin signaling is beneficial to retard the IRI-induced AKI-to-CKD continuum.

TGF-β1 can drive EMT of several types of cells, promote excessive ECM production, and inhibit ECM degradation suppression.[39] The TGF-β pathway currently divides into a Smad-dependent and a Smad-independent pathway. In the TGF-β/Smad pathway, active TGF-β1 binds to TGFβRII, then recruits TGFβRI and phosphorylates downstream Smad2 and Smad3, which are extensively activated in the fibrotic kidney with CKD.[40] Within the Smads family, Smad3 plays a decisive role due to direct binding to the promoter region of collagens to trigger their production.[1] Smad4 participates in the nucleocytoplasmic shuttling of Smad2/3 complexes, while Smad7 is a negative regulator of the TGF-β/Smad pathway. Smad3 directly induces Smad7 production, while Smad7

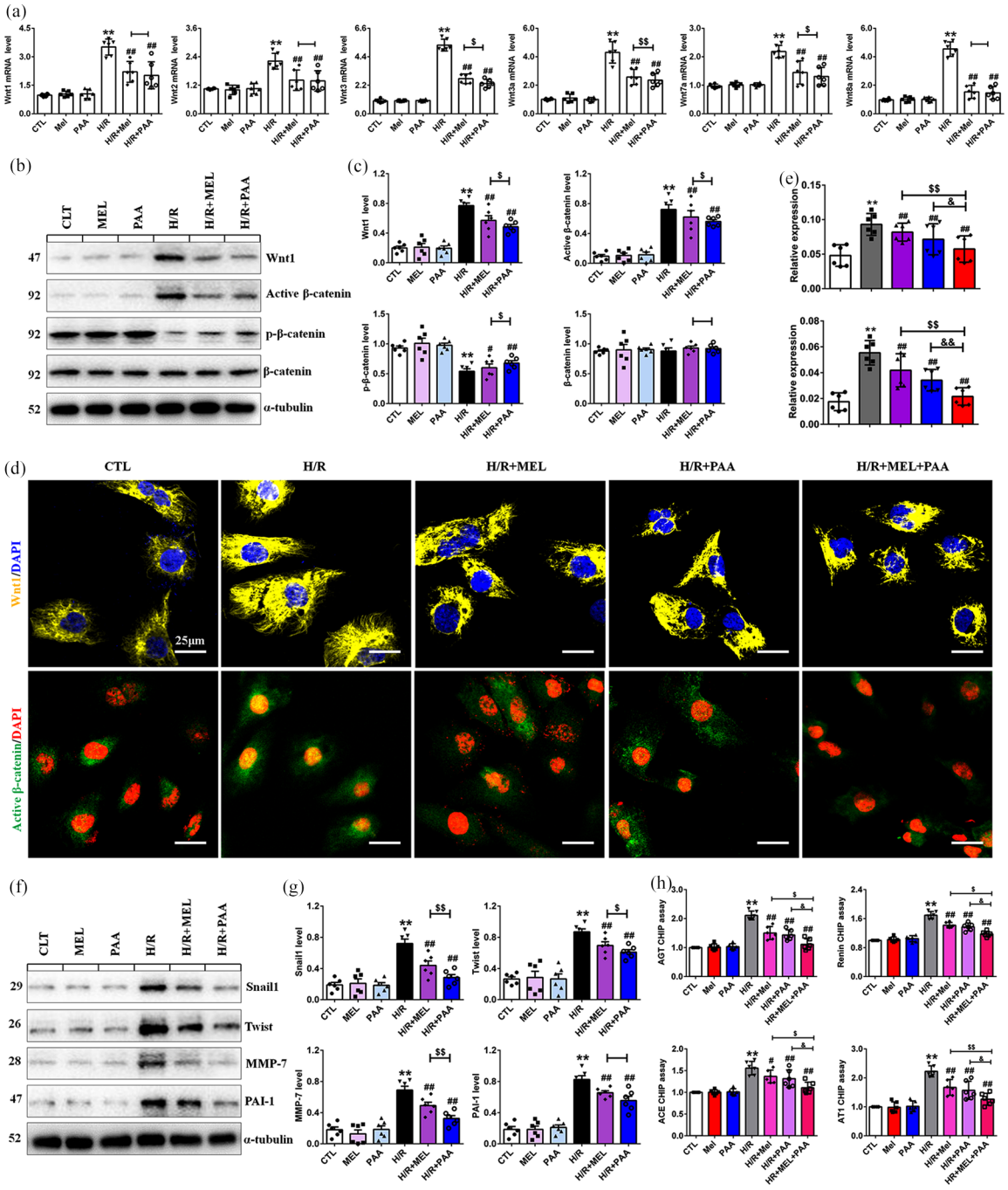

Figure 6. Inhibitory effect of melatonin and PAA against the activation of Wnt/β-catenin pathway *in vitro*. (a) The mRNA levels of Wnt1, Wnt2, Wnt3, Wnt3a, Wnt7a, and Wnt8a in different groups. (b, c) Protein levels of Wnt1, active β-catenin, p-β-catenin, and β-catenin in indicated groups. (d, e) Immunofluorescence staining of Wnt1 (yellow) and active β-catenin (green) in indicated groups. Scale bar, 25 μm. (f, g) Protein levels of snail1, twist, MMP-7 and PAI-1 in indicated groups. (h) ChIP assay results of AGT, renin, ACE and AT1R in different groups. Data represented as mean ± SD ($n = 6$).

ACE, Angiotensin-converting enzyme; AGT angiotensinogen, AT1R, angiotensin II type 1 receptor; ChIP, chromatin immunoprecipitation; MMP-7, matrix metalloproteinase-7; PAA, poricoic acid A; PAI-1, plasminogen activator inhibitor-1. $^{**}p < 0.01$ *versus* CTL; $^{\#}p < 0.05$; $^{\#\#}p < 0.01$ *versus* H/R group; $^{\$}p < 0.05$; $^{\$\$}p < 0.01$ *versus* H/R + melatonin group; $^{\&}p < 0.05$; $^{\&\&}p < 0.01$ *versus* H/R + PAA group.

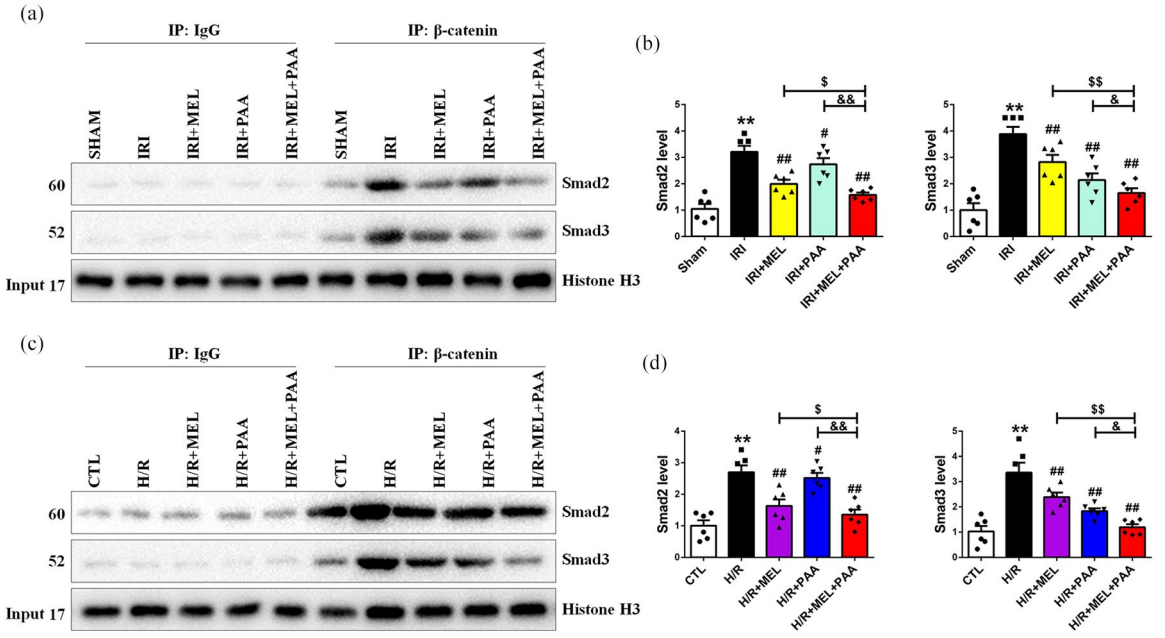

Figure 7. PAA enhanced the effect of melatonin on the interaction of Smad3 and β-catenin signaling. (a, b) Co-IP bands of Smad2 and Smad3 in indicated groups at day 14 after the IRI procedure. (c, d) Co-IP bands of Smad2 and Smad3 in indicated groups. Data represented as mean ± SD ($n = 6$).
Co-IP, Coimmunoprecipitation; IRI, ischemia-reperfusion injury; PAA, poricoic acid A.
$^{**}p < 0.01$ *versus* CTL; $^{\#}p < 0.05$; $^{\#\#}p < 0.01$ *versus* H/R group; $^{\$}p < 0.05$; $^{\$\$}p < 0.01$ *versus* IRI + melatonin or H/R + melatonin group; $^{\&}p < 0.05$; $^{\&\&}p < 0.01$ *versus* H/R + PAA group.

contributes to the degradation of Smad3.[14] In this study, renal IRI significantly induced the upregulation of TGF-β1 at both mRNA and protein levels during the AKI-to-CKD continuum. The increase of TGF-β1 resulted in the upregulation of p-Smad2, p-Smad3, and Smad4, as well as the downregulation of Smad7. Treatment with melatonin significantly reduced the upregulation of p-Smad2, p-Smad3, and Smad4, as well as increasing Smad7 expression. However, PAA showed different inhibitory effects from melateonin. PAA selectively inhibited the phosphorylation of Smad3 but did not affect other mediators. Similar results were observed from H/R and TGF-β1-induced HK-2 cells. Co-IP data also demonstrated that melatonin blocked the interactions of Smad2 and Smad3 with TGFβRI and SARA, while PAA specifically suppressed the interactions of Smad3 with TGFβRI and SARA, and PAA had a greater inhibitory effect than melatonin on the phosphorylation of Smad3. After knockdown of Smad3, the effects of PAA and melatonin were significantly weakened, partially owing to the loss of their therapeutic targets. Promoter assay results indicated that both melatonin and PAA mitigated IRI-induced Smad3-dependent collagen I promoter activity, while PAA showed a stronger inhibitory effect than melatonin. Taken together, melatonin showed extensive inhibitory effects on Smad signaling, while PAA selectively suppressed the phosphorylation of Smad3 and had a greater inhibitory effect than melatonin on p-Smad3.

The Smad-independent pathway was examined further. IRI and H/R led to the upregulation of p-PI3K, p-ERK1/2, and p-p38. Melatonin significantly reduced the upregulation of p-PI3K, p-ERK1/2, and p-p38, while PAA hardly affected these downstream mediators during the AKI-to-CKD continuum. Although both melatonin and PAA treatment exhibited good renoprotective and antifibrotic effects, the underlying mechanisms of these two agents were totally different. Melatonin could simultaneously target multiple downstream mediators of TGF-β1 to reduce fibrogenesis, while PAA performed an entirely different mechanism that selectively inhibited the phosphorylation of Smad3.

In normal adult kidney, Wnt/β-catenin is silent. Once the kidney suffers injury, Wnt/β-catenin signaling is activated and induces the upregulation of downstream targets, most of which are associated with fibrogenesis.[20] The level of β-catenin controls both activation of this pathway and downstream gene expression.[41] In the absence of Wnt ligands, β-catenin is phosphorylated and subsequently degraded by the proteasome. In the presence of Wnts, the degradation of β-catenin is inhibited, resulting in β-catenin dephosphorylation and stabilization. β-Catenin accumulates in the cytoplasm and transfers into the nucleus,[42] which initiates transcription of target genes, including snail1, twist, PAI-1, and MMP–7. Snail1 and twist promote fibrogenesis in the kidney.[43] Snail1 expression reduces E-cadherin expression and further disrupts cell-to-cell adhesion in epithelial cells, which is the initiation of EMT.[44] PAI-1 contributes to CKD progress.[18] The upregulation of MMP-7 results in the shedding of E-cadherin and promotes cell apoptosis and death.[45] The expression of several Wnts were upregulated at 3 and 14 days in IRI rats, which was accompanied by upregulation of active β-catenin and downregulation of p-β-catenin protein, indicating activation of the Wnt/β-catenin pathway during the AKI-to-CKD continuum. Activation of the Wnt/β-catenin pathway resulted in upregulation of snail1, twist, PAI-1, and MMP-7 in IRI rats and H/R-induced HK-2 cells. Melatonin and PAA reduced the upregulation of Wnt1 and active β-catenin, and restored the downregulation of p-β-catenin during the AKI-to-CKD continuum. The upregulation of snail1, twist, PAI-1, and MMP-7 were also attenuated by melatonin and PAA treatment. Melatonin and PAA transcriptionally suppressed expression of snail1, twist, PAI-1, and MMP–7. Inhibition of the Wnt/β-catenin pathway by melatonin and PAA also retarded the expression of RAS components. Although both melatonin and PAA inhibited the Wnt/β-catenin pathway, PAA showed a stronger inhibitory effect than melatonin during the AKI-to-CKD continuum.

Additionally, the interaction exists in TGF-β/Smad and Wnt/β-catenin pathways. TGF-β1 contributes to β-catenin accumulation in the cytoplasm and the combination with TCF/LEF in the nucleus to initiate the expression of profibrotic factors and induce fibrosis.[46] TGF-β1 also induces β-catenin/Smad3 complex to enhance Smad3-induced fibrosis.[47] Inhibition of the β-catenin/Smad3 complex weakens TGF-β-induced fibrosis.[47] In this study, we found that IRI and H/R enhanced the interaction of Smad2/3 and β-catenin, which accelerated renal fibrosis. Melatonin disturbed the interactions of Smad2 and Smad3 with β-catenin, while PAA selectively affected the interaction of Smad3 with β-catenin. Notably, PAA enhanced melatonin's effects to inhibit the interaction of Smad2 and β-catenin, while melatonin enhanced the effects of PAA in inhibiting the interaction of Smad3 and β-catenin. These results point to the synergetic effects underlying the mechanisms of PAA and melatonin against renal fibrosis (Figure 8). Both melatonin and PAA have the potential to be developed as new agents against renal fibrosis.

Our current study has several limitations. Here, we found that CKD contributed to the interaction of Smad3 and β-catenin during the AKI-to-CKD continuum, and melatonin and PAA treatment significantly weakened this interaction. However, the inhibitory effects of combined melatonin and PAA therapy against other profibrotic signal pathways, including interleukin, hedgehog, and the connective tissue growth factor pathway, were not detected, which may suggest their involvement in the therapeutic effects of combined therapy. Additionally, a mouse model was not used. However, the positive results from the human cell line and rat model suggested possible generalization of renoprotection by melatonin and PAA in different species.

In conclusion, our study demonstrated that combined therapy with melatonin and PAA led to better antifibrotic effects than either compound used alone in renal IRI rats and H/R-induced HK-2 cells. Melatonin and PAA could prevent the AKI-to-CKD continuum by inhibition of the TGF-β/Smad and Wnt/β-catenin pathways. However, their underlying mechanisms were different. Melatonin exhibited extensive inhibitory effects, while PAA selectively inhibited the phosphorylation of Smad3. Melatonin and PAA treatment also disturbed the interaction of the TGF-β/Smad and Wnt/β-catenin pathways. These results strongly support the effects of melatonin and PAA against renal fibrosis, and provide a candidate strategy to slow down the AKI-to-CKD continuum.

Funding

The author(s) disclosed receipt of the following financial support for the research, authorship,

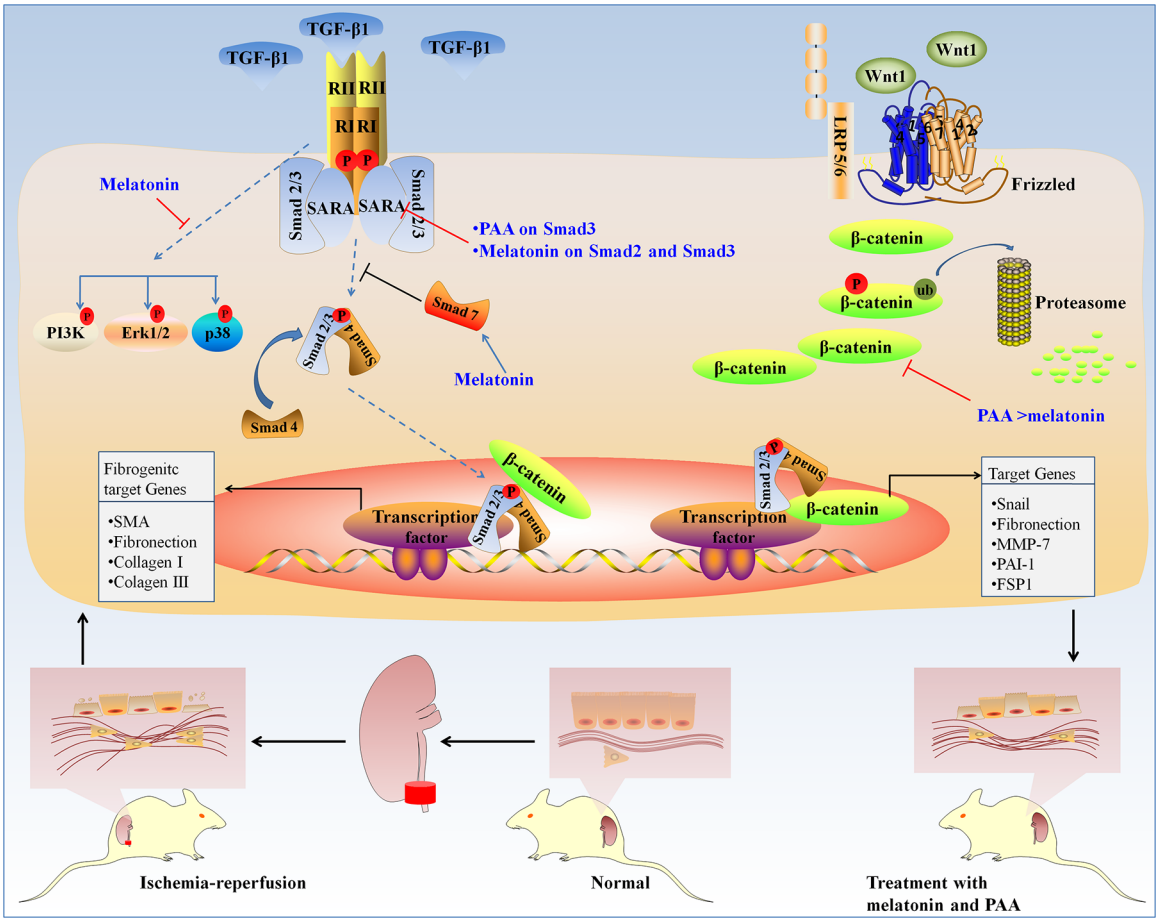

Figure 8. Schematic diagram depicting possible mechanisms involved in the anti-fibrotic effect of melatonin and PAA. Renal IRI activated TGF-β signaling and caused renal fibrosis. Treatment with both melatonin and PAA simultaneously inhibit renal fibrosis, but the underlying mechanisms are totally different. Melatonin treatment targets multiple downstream mediators of TGF-β signaling, including Smad2, Smad3, Smad4, Smad7, PI3K, ERK1/2, and p38, while PAA treatment attenuates renal fibrosis by selectively inhibiting Smad3 phosphorylation *via* disturbing the interactions of Smad3 with TGFβRI and SARA. Interestingly, PAA treatment can enhance the inhibitory effects of melatonin on Smad2 and Smad3 phosphorylation. Besides, PAA has greater inhibitory effects than melatonin on the activation of Wnt/β-catenin signaling and downstream target genes.

IRI, ischemia-reperfusion injury; PAA, poricoic acid A; PAI-1, plasminogen activator inhibitor-1; SARA, Smad anchor for receptor activation; TGF-β, transforming growth factor-β, TGFβRI, transforming growth factor-β receptor II.

and publication of this article: This study was supported by the National Natural Science Foundation of China (Nos. 81872985, 81673578), and NWU Graduate Innovation and Creativity Funds (YZZ17157). No funding bodies had any role in study design, data collection, and analysis, decision to publish, or preparation of the manuscript.

Conflict of interest statement

The author(s) declared no potential conflicts of interest with respect to the research, authorship, and/or publication of this article.

ORCID iD

Ying-Yong Zhao https://orcid.org/0000-0002-0239-7342

Supplemental material

Supplemental material for this article is available online.

References

1. Chen L, Yang T, Lu DW, *et al.* Central role of dysregulation of TGF-β/Smad in CKD progression and potential targets of its treatment. *Biomed Pharmacother* 2018; 101: 670–681.

2. Takaori K and Yanagita M. Insights into the mechanisms of the acute kidney injury-to-chronic kidney disease continuum. *Nephron* 2016; 134: 172–176.
3. Chen D, Cao G, Chen H, *et al*. Identification of serum metabolites associating with chronic kidney disease progression and anti-fibrotic effect of 5-methoxytryptophan. *Nat Commun* 2019; 10: 1476.
4. Chawla LS and Kimmel PL. Acute kidney injury and chronic kidney disease: an integrated clinical syndrome. *Kidney Int* 2012; 82: 516–524.
5. Chen YY, Chen DQ, Chen L, *et al*. Microbiome–metabolome reveals the contribution of gut–kidney axis on kidney disease. *J Transl Med* 2019; 17: 5.
6. Chen L, Chen DQ, Liu JR, *et al*. Unilateral ureteral obstruction causes gut microbial dysbiosis and metabolome disorders contributing to tubulointerstitial fibrosis. *Exp Mol Med* 2019; 51: 38.
7. Xiao L, Zhou D, Tan RJ, *et al*. Sustained activation of Wnt/β-catenin signaling drives AKI to CKD progression. *J Am Soc Nephrol* 2016; 27: 1727–1740.
8. Li Z, Zhou L, Wang Y, *et al*. (Pro)renin Receptor is an amplifier of Wnt/β-catenin signaling in kidney injury and fibrosis. *J Am Soc Nephrol* 2017; 28: 2393–2408.
9. Yip HK, Yang CC, Chen KH, *et al*. Combined melatonin and exendin-4 therapy preserves renal ultrastructural integrity after ischemia-reperfusion injury in the male rat. *J Pineal Res* 2015; 59: 434–447.
10. Chen DQ, Feng YL, Chen L, *et al*. Poricoic acid A enhances melatonin inhibition of AKI-to-CKD transition by regulating Gas6/Axl-NF-κB/Nrf2 axis. *Free Radic Biol Med* 2019; 134: 484–497.
11. Yang F, Huang XR, Chung AC, *et al*. Essential role for Smad3 in angiotensin II-induced tubular epithelial-mesenchymal transition. *J Pathol* 2010; 221: 390–401.
12. Chen DQ, Cao G, Chen H, *et al*. Gene and protein expressions and metabolomics exhibit activated redox signaling and wnt/β-catenin pathway are associated with metabolite dysfunction in patients with chronic kidney disease. *Redox Biol* 2017; 12: 505–521.
13. Chen DQ, Chen H, Chen L, *et al*. The link between phenotype and fatty acid metabolism in advanced chronic kidney disease. *Nephrol Dial Transplant* 2017; 32: 1154–1166.
14. Meng XM, Tang PM, Li J, *et al*. TGF-β/Smad signaling in renal fibrosis. *Front Physiol* 2015; 6: 82.
15. Wang M, Chen DQ, Wang MC, *et al*. Poricoic acid ZA, a novel RAS inhibitor, attenuates tubulo-interstitial fibrosis and podocyte injury by inhibiting TGF-β/Smad signaling pathway. *Phytomedicine* 2017; 36: 243–253.
16. Morishita Y, Yoshizawa H, Watanabe M, *et al*. siRNAs targeted to Smad4 prevent renal fibrosis in vivo. *Sci Rep* 2014; 4: 6424.
17. Meng XM, Huang XR, Xiao J, *et al*. Disruption of Smad4 impairs TGF-β/Smad3 and Smad7 transcriptional regulation during renal inflammation and fibrosis *in vivo* and *in vitro*. *Kidney Int* 2012; 81: 266–279.
18. Tan RJ, Zhou D, Zhou L, *et al*. Wnt/β-catenin signaling and kidney fibrosis. *Kidney Int Suppl* 2014; 4: 84–90.
19. Zhou L, Li Y, Hao S, *et al*. Multiple genes of the renin-angiotensin system are novel targets of Wnt/β-catenin signaling. *J Am Soc Nephrol* 2015; 26: 107–120.
20. Dai B, Wu Q, Zeng C, *et al*. The effect of Liuwei Dihuang decoction on PI3K/Akt signaling pathway in liver of type 2 diabetes mellitus (T2DM) rats with insulin resistance. *J Ethnopharmacol* 2016; 192: 382–389.
21. Chen DQ, Chen H, Chen L, *et al*. Metabolomic application in toxicity evaluation and toxicological biomarker identification of natural product. *Chem Biol Interact* 2016; 252: 114–130.
22. Chen DQ, Hu HH, Wang YN, *et al*. Natural products for the prevention and treatment of kidney disease. *Phytomedicine* 2018; 50: 50–60.
23. Hu HH, Chen DQ, Wang YN, *et al*. New insights into TGF-β/Smad signaling in tissue fibrosis. *Chem Biol Interact* 2018; 292: 76–83.
24. Chen L, Cao G, Wang M, *et al*. The Matrix Metalloproteinase-13 inhibitor poricoic acid ZI ameliorates renal fibrosis by mitigating epithelial–mesenchymal transition. *Mol Nutr Food Res* 2019; e1900132.
25. Zhao YY, Feng YL, Bai X, *et al*. Ultra performance liquid chromatography-based metabonomic study of therapeutic effect of the surface layer of *Poria cocos* on adenine-induced chronic kidney disease provides new insight into anti-fibrosis mechanism. *PLoS One* 2013; 8: e59617.
26. Zhao YY, Li HT, Feng YI, *et al*. Urinary metabonomic study of the surface layer of *Poria cocos* as an effective treatment for chronic renal injury in rats. *J Ethnopharmacol* 2013; 148: 403–410.

27. Zhao YY, Lei P, Chen DQ, *et al*. Renal metabolic profiling of early renal injury and renoprotective effects of *Poria cocos* epidermis using UPLC Q-TOF/HSMS/MS^{E}. *J Pharm Biomed Anal* 2013; 81–82: 202–209.
28. Zhao YY, Feng YL, Du X, *et al*. Diuretic activity of the ethanol and aqueous extracts of the surface layer of *Poria cocos* in rat. *J Ethnopharmacol* 2012; 144: 775–778.
29. Feng YL, Lei P, Tian T, *et al*. Diuretic activity of some fractions of the epidermis of *Poria cocos*. *J Ethnopharmacol* 2013; 150: 1114–1118.
30. Wang M, Chen DQ, Chen L, *et al*. Novel RAS inhibitors poricoic acid ZG and poricoic acid ZH attenuate renal fibrosis *via* Wnt/β-catenin pathway and targeted phosphorylation smad3 signaling. *J Agric Food Chem* 2018; 66: 1828–1842.
31. Yoon JJ, Lee YJ, Lee SM, *et al*. Oryeongsan suppressed high glucose-induced mesangial fibrosis. *BMC Complement Altern Med* 2015; 15: 30.
32. Wang YZ, Zhang J, Zhao YL, *et al*. Mycology, cultivation, traditional uses, phytochemistry and pharmacology of *Wolfiporia cocos* (Schwein.) Ryvarden et Gilb.: a review. *J Ethnopharmacol* 2013; 147: 265–276.
33. Hu W, Ma Z, Jiang S, *et al*. Melatonin: the dawning of a treatment for fibrosis? *J Pineal Res* 2016; 60: 121–131.
34. dos Santos M, Favero G, Bonomini F, *et al*. Oral supplementation of melatonin protects against lupus nephritis renal injury in a pristane-induced lupus mouse model. *Life Sci* 2018; 193: 242–251.
35. Ishigaki S, Ohashi N, Matsuyama T, *et al*. Melatonin ameliorates intrarenal renin–angiotensin system in a 5/6 nephrectomy rat model. *Clin Exp Nephro* 2018; 22: 539–549.
36. Chen H, Cao G, Chen DQ, *et al*. Metabolomics insights into activated redox signaling and lipid metabolism dysfunction in chronic kidney disease progression. *Redox Biol* 2016; 10: 168–178.
37. Chen H, Yang T, Wang MC, *et al*. Novel RAS inhibitor 25-O-methylalisol F attenuates epithelial-to-mesenchymal transition and tubulo-interstitial fibrosis by selectively inhibiting TGF-β-mediated Smad3 phosphorylation. *Phytomedicine* 2018; 42: 207–218.
38. Ai J, Nie J, He J, *et al*. GQ5 hinders renal fibrosis in obstructive nephropathy by selectively inhibiting TGF-β-Induced Smad3 phosphorylation. *J Am Soc Nephrol* 2015; 26: 1827–1838.
39. Chen DQ, Feng YL, Cao G, *et al*. Natural products as a source for antifibrosis therapy. *Trends Pharmacol Sci* 2018; 39: 937–952.
40. Meng XM, Chung Arthur CK and Lan Hui Y. Role of the TGF-β/BMP-7/Smad pathways in renal diseases. *Clin Sci* 2013; 124: 243–254.
41. MacDonald BT, Tamai K and He X. Wnt/β-catenin signaling: components, mechanisms, and diseases. *Dev cell* 2009; 17: 9–26.
42. Nusse R and Clevers H. Wnt/β-catenin signaling, disease, and emerging therapeutic modalities. *Cell* 2017; 169: 985–999.
43. Lovisa S, LeBleu VS, Tampe B, *et al*. Epithelial-to-mesenchymal transition induces cell cycle arrest and parenchymal damage in renal fibrosis. *Nat Med* 2015; 21: 998–1009.
44. Li Y, Wen X and Liu Y. Tubular cell dedifferentiation and peritubular inflammation are coupled by the transcription regulator Id1 in renal fibrogenesis. *Kidney Int* 2012; 81: 880–891.
45. Tan RJ and Liu Y. Matrix metalloproteinases in kidney homeostasis and diseases. *Am J Physiol Renal Physiol* 2012; 302: F1351–F1361.
46. Zheng G, Lyons JG, Tan TK, *et al*. Disruption of E-cadherin by matrix metalloproteinase directly mediates epithelial-mesenchymal transition downstream of transforming growth factor-β1 in renal tubular epithelial cells. *Am J Pathol* 2009; 175: 580–591.
47. Tian X, Zhang J, Tan TK, *et al*. Association of β-catenin with P-Smad3 but not LEF-1 dissociates in vitro profibrotic from anti-inflammatory effects of TGF-β1. *J Cell Sci* 2013; 126: 67–76.